

Modelling and Validation of the Mechatronic Wedge Brake

Richard Roberts, Martin Schautt, Henry Hartmann & Bernd Gombert

eStop GmbH, An der Hartmühle 10, 82229 Seefeld, Germany

Copyright © 2003 SAE International

ABSTRACT

The eBrake[®] is a novel self-reinforcing electro-mechanical wedge brake^[1]. Self reinforcement reduces the actuation forces, resulting in a more efficient and smaller brake, but demands more precise control than a conventional braking system. As a result, mathematical modelling and control law development plays a significant role in the development process.

This paper describes the mathematical model of the brake and its validation against the prototype hardware. It is shown that there is a good correspondence between theory and practice, demonstrating both the validity of the model and its potential as a tool in future developments. Both the model and test results illustrate that the potential advantages of this design are realisable in practice.

INTRODUCTION

In both the automotive and aerospace industries today, there is a strong trend towards 'power-by-wire' technologies, aimed at replacing hydraulic or pneumatic systems with equivalent electrically powered ones. Accordingly, there has been interest for some years in electrically actuated brakes and several companies have designed and tested prototype systems.

In floating calliper brakes, production of a braking moment relies on the generation of a large clamping force between two or more brake pads, which then produce a frictional torque on the rotating assembly. For electric brake actuators, the clamping force is typically generated by coupling a motor through a gearbox onto a ball- or roller-screw. The actuator output bearings must support the worst case clamping load. By definition, for the motor to produce a torque a current is required, resulting in a constant power drain. In practice, a compromise has to be found between the high gear ratio needed to minimise the current for continuous braking and the low gear ratio which minimises the current for dynamics.

It would clearly be of benefit if the force required from the brake actuator could be reduced, since this would make this compromise much easier to reach. The eBrake[®] solves this problem elegantly by using a wedge to

generate the clamping forces. This exploits self-reinforcement of the braking forces by the rotating brake disc to minimise the actuation forces. At the ideal operating point, where the coefficient of friction is equal to the tangent of the wedge angle, the steady-state actuation force required to generate any braking torque is zero. Mathematically, the characteristic brake factor for a floating calliper brake actuated by this method is given by^[1]

$$C^* = \frac{\text{Pad Braking Force}}{\text{Brake Actuation Force}} = \frac{2\mu_B}{\tan \alpha - \mu_B}$$

From this equation, it can be seen that for low coefficients of friction, C^* is positive, so a steady pushing force is required to maintain the braking force. When the coefficient of friction is greater than the tangent of the wedge angle, then a steady pulling force is required from the actuator to stop the wedge being pulled further in.

For optimum performance, it is best to operate around the point at which the characteristic brake factor is infinite, since this minimises the control forces required. From a control standpoint, this can be thought of as a point of neutral stability, since any small perturbation in the wedge position will result in it remaining in the new position (and generating the corresponding braking moment). When the coefficient of friction increases, the wedge position becomes unstable and needs to be controlled to stop the wheel jamming.

As a result of this instability, it is important to develop an adequate mathematical model of the brake system prior to testing the hardware. This serves several functions:

- To assist in understanding the system;
- To help develop suitable control laws;
- To allow virtual testing of the hardware.

In practice, several different models may be developed, with a level of complexity appropriate to the problem to be investigated.

One of the most important aspects of producing an appropriate model of the brake is the consideration of friction. Most obviously, the friction between the brake pads and brake disc is a fundamental parameter in the

brake torque control. Any controller must be sufficiently robust to this parameter to avoid producing undesirable responses or even instability. Secondly, the mechanical friction within the various components is also important, since it can potentially increase power losses and degrade the performance of the controller. Friction terms will be mentioned wherever they occur in the model.

The objective of this paper is to show how the brake has been modelled and to compare the simulation results with the test results. It is divided into six main sections containing:

- A brief description of the current prototype;
- Presentation of the equations used for modelling the individual components;
- A short description of the tests used to generate key modelling data;
- Comparison of simulation and test results;
- eBrake[®] programme status;
- Conclusions.

Further details of the underlying concept and references to the some of the underlying patents are provided in Reference 1.

SYSTEM DESCRIPTION

The test stand including the prototype system is illustrated in Figure 1. It consists of an A.C. motor driving a flywheel, which is attached to the brake disc. The test brake is based on a floating calliper arrangement mounted around the brake disc. It is attached to earth via a moment sensor which measures the applied torque.

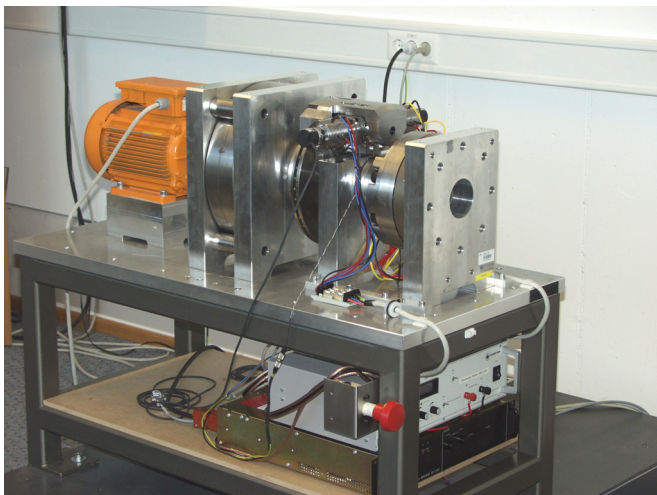


Figure 1: Test Stand with Prototype

A section through the CAD model is presented in Figure 2, which provides a better view of the internal workings of the brake. The existing design is based around a modular concept suitable for laboratory testing, rather than being optimised for minimum volume and weight, and uses off-the-shelf commercial components wherever possible.

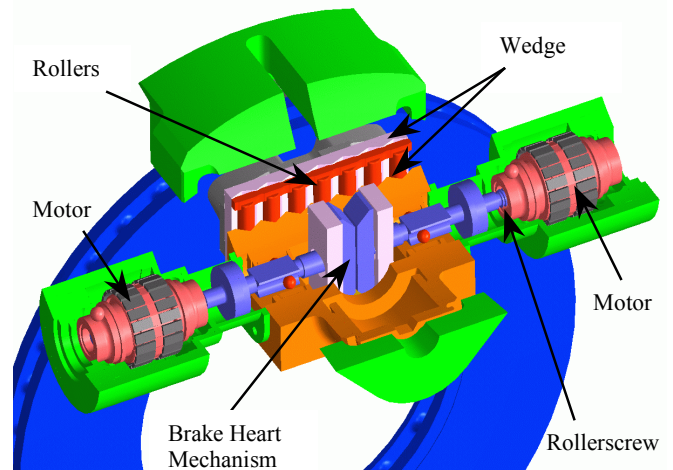


Figure 2. Cross Section through Prototype

The motive power is provided by two brushless permanent magnet D.C. motors, mounted at either end of the assembly. Each of these consists of two stators from the DLR ILM-50 motor^[2], mounted in parallel, driving a specially constructed rotor. The motor rotation is converted to linear motion by means of roller-screws. Their nuts are mounted within the motor rotors on preloaded angular thrust ball bearings, with sufficient preload to resist all the linear operating loads. The roller-screws drive the so-called brake heart, which contains the wedge mechanism.

Within the brake heart mechanism, forces are only transmitted by compression between neighbouring surfaces. This allows the motors either to work together or to preload the system. If they are working together, then there is contact between one roller-screw drive surface and the wedge. The other roller-screw pushes against the first roller-screw. This reduces the motor loads when the coefficient of friction is not near the optimum value ($\tan \alpha$). For a preload to be introduced, both roller-screws contact their respective sides of the wedge. This possibility is required so that free-play can be removed when the coefficient of friction is close to the ideal value^[3]. Backlash is inevitable, both as a result of construction tolerances and due to wear, principally in the bearing surface which allows the outer part of the wedge to slide outwards from the motor axis.

The wedge is actually composed of two ground 'W' surfaces, the inner of which relative to the motors is static, and the outer of which moves both axially and in translation. This construction spreads the loads and allows the brake to use self-reinforcement in both directions of rotation. Between these surfaces, there is a series of rollers, which serve primarily to minimise the sliding friction, since the forces normal to the brake disc will be as high as in a conventional brake. The outer part of the wedge, to which the brake pad is attached, is held against the static one by a preloaded spring. It is actuated via a bearing surface, which allows it to move laterally away from the motor centreline.

Commutation and current control of the motors is performed using commercial motor drives with an incremental encoder on each motor shaft. For controlled braking, a moment sensor provides the feedback to the moment controller, which is implemented in the dSPACE development environment. Alternatively, the encoder can be used to provide motor position control.

COMPONENT MODELLING

For the purposes of modelling, it is convenient to subdivide the brake into a number of different assemblies. These can be implemented as separate subroutines or blocks within the overall model.

CURRENT CONTROLLER

The current controller is a relatively simple model. The input demand is passed through a first order filter and limited to the value set in the hardware. The actual motor current is 'sensed' using a representative high frequency filter and then scaled appropriately to be compared with the demand value. The current error is then used as the input to the proportional plus integral controller. The output from this is scaled by a PWM gain, which is dependent on and limited to the supply voltage, to produce the motor input voltage.

Since the PWM frequency used is 40 kHz, no attempt has been made to model it in detail. To date, it has also not been found necessary to consider small amplitude non-linearities in this system.

MOTOR

The motor is modelled using the standard equations for permanent magnet D.C. motors. Broadly speaking, the input voltage is used to establish the motor current, which produces a corresponding torque. This is summed with all the other torques acting on the rotor to produce an accelerating torque, from which the motor acceleration can be determined. By integration, it is then possible to calculate the rotor speed and position.

Briefly reviewing the equations, the motor current is determined from

$$V_{IN} = i_M R_M + L_M \frac{di_M}{dt} + K_T \omega_M$$

$$\Rightarrow \frac{di_M}{dt} = \frac{1}{L_M} (V_{IN} - i_M R_M - K_T \omega_M)$$

Integration can be used to give the instantaneous motor current. Note that the motor back-emf term uses the motor torque constant – this is correct as long as its units are Nm/A, and the motor speed is expressed in radians/second.

The motor speed can be calculated using

$$J_M \frac{d\omega_M}{dt} = T_M + T_{COG} + T_{SCREW} - T_{DAMP} - T_{FRICT}$$

$$\Rightarrow \dot{\omega}_M = \frac{1}{J_M} (K_T i_M + T_{COG} + T_{SCREW} - D_M \omega_M - T_{FRICT})$$

The cogging torque was modelled and matched to test results but was not found to play a major role in the dynamics compared to other effects. The torque from the roller-screw and the friction losses are discussed in the next sub-section. The motor inertia used includes the inertias of all the components mounted on the shaft: the motor rotor, encoder, roller-screw, and bearings.

ROLLERSCREW & BEARINGS

There are several issues to be addressed in the modelling of the roller screw. Firstly, there is the conversion of motor torque to axial force (and vice-versa, since the screw can be back-driven). Secondly, there are losses within the screw to consider, and finally there are frictional losses within the bearings. The roller-screw and bearings are considered mass-less, and it is only the torques and forces that are of interest. These are used to determine the motor acceleration, as described above.

Considering the screw first, then if there are no losses, the axial force is calculated from

$$F_{SCREW} = \frac{2\pi}{L} T_{SCREW}$$

In practice, the roller-screw will have a certain efficiency, which may be dependent on whether it is driving or being back-driven. This is both the result of, and can be modelled as, friction within the screw. Working only in torque, then

$$T_{LOSS} = (1 - \eta) \times T_{DRIVE}$$

This acts as a friction which must be overcome for an accelerating torque to remain on the other side of the transmission.

The bearing torques are dependent on two main factors:

- axial load;
- shaft speed.

The friction is calculated based on experience with similar bearing arrangements and information from the roller-screw catalogue^[4]. Taking the terms in turn:

$$T_{FRICT_AXIAL} \approx C_0 + C_1 F_{AXIAL} + C_2 F_{AXIAL}^2$$

The constant term represents the moment due to the bearing preload on the otherwise unloaded shaft. The first order term is essentially zero since the arrangement

is symmetric, and the quadratic term is an approximation to the effect of unloading one bearing and loading the other as the axial load is applied.

The shaft speed manifests itself in two terms, one due to the oil viscosity and the other from the Stribeck effect.

$$T_{FRICT_{SPEED}} = G_v (v\omega_M)^{k_v} + G_S e^{-k_S \frac{\omega_M}{\omega_S}} T_{FRICT_{AXIAL}}$$

In practice, with the arrangement described, these effects have not had a major influence on the results.

The total friction on the motor shaft is the sum of all these effects.

BRAKE HEART

A schematic diagram of the Brake Heart model is shown in Figure 3.

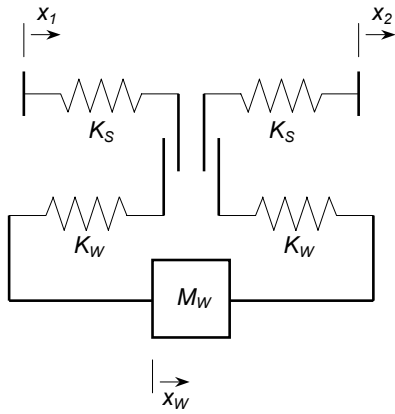


Figure 3. Schematic of Brake Heart Model

The model includes several main terms:

- Axial stiffness of the roller-screw and bearings;
- Axial stiffness of the wedge to roller-screw interfaces;
- Mass of the moving component of the wedge;
- Free-play between roller-screws and wedge;
- Free-play between the two roller-screws.

A small amount of damping is included with each of the spring terms to prevent unrealistic oscillation of the wedge.

The diagram shows clearly how the brake heart functions. The wedge can only be driven by means of compression across the roller-screw to wedge interface. The motors screws are free to work with or against each other, either coupled through the wedge or pushing directly on each other.

Although the frequency of the wedge mass oscillating against the roller-screw springs is relatively high, it is important to include the flexibility correctly because it

affects both the control loop and the magnitude of any force-fight between the two motors.

The equations for this system are relatively trivial, based as they are on the differences in position and rate between the various elements. The main simulation issue is establishing exactly when the different elements are actually in contact. The axial forces which result are applied to the two motors and to the wedge itself.

From this simplified diagram, it is not immediately apparent that there is friction across the wedge to roller-screw interface which resists the lateral motion of the wedge. For simplicity, this can be resolved into the linear direction and treated as a friction acting linearly on the wedge. Consideration of the geometry gives

$$F_{FRICT_{INT}} = \mu_{INT} F_{INT} \tan \alpha$$

By combining this with the overall axial force from the motors and adding the forces due to braking, it is possible to integrate for the axial position of the wedge.

WEDGE AND BRAKE CALLIPER

The forces developed in the wedge and calliper are applied to two systems: the wedge and the braked flywheel. The equations will first be developed ignoring any friction within the assembly to clarify the underlying behaviour. For simplicity, it will be assumed that the point of contact is at a displacement of zero, although clearance means that this will not be the case. Considering the geometry shown in Figure 4, then the force normal to the brake disc is

$$F_N = K_{CAL} x_W \tan \alpha$$

Assuming that the disc is rotating, the braking force is

$$F_B = \mu_B F_N = \mu_B K_{CAL} x_W \tan \alpha$$

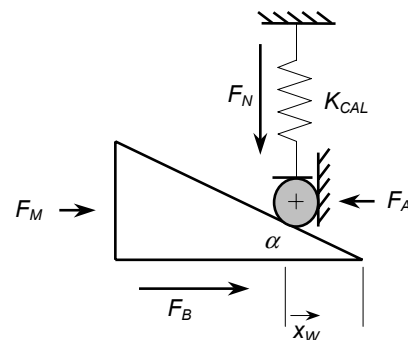


Figure 4. Forces on Wedge

Due to the wedge angle, there is a component of the reaction force in the axial direction. This is given by

$$F_A = -F_N \tan \alpha$$

Thus the total axial force acting on the wedge is

$$\begin{aligned} F_W &= (\mu_B - \tan \alpha) F_N + F_M \\ &= (\mu_B - \tan \alpha) K_{CAL} x_W \tan \alpha + F_M \end{aligned}$$

A simple model of the friction in the rollers can also be implemented in the form

$$F_{FRICT_W} = \mu_R F_N$$

The coefficient of friction was initially set to a pessimistic value for design studies, but it has subsequently been reduced. Note that self-reinforcement only functions while the wheel is turning. Once it has stopped, then the axial force on the wedge is given by

$$F_W = -K_{CAL} x_W \tan^2 \alpha + F_M$$

Finally, the braking torque is given by using the pads on both sides of the calliper and multiplying by their effective radius, such that

$$M_B = 2\mu_B F_N r_B$$

This is applied as a decelerating torque to the flywheel.

INITIAL TESTS

Prior to conducting detailed comparisons between the model and hardware, tests were required to provide the necessary data. The main objectives of these tests were to:

- Calibrate sensors
- Check the motor current loop model
- Check calculated component masses and inertias
- Measure roller-screw efficiency
- Measure drive train stiffnesses

Sensor calibration is an obvious necessity and will not be further discussed. Similarly, measuring the component masses is a routine exercise which does not require explanation. However, the other issues will be briefly addressed.

MOTOR CURRENT LOOP

The motor drive manufacturer provided some modelling data for the hardware used. Testing is still important for establishing confidence in this model, even though the bandwidth is very high and interference with other parts of the control loop should be minimal. This saves time later if unexpected results occur.

By exploiting the fact that each motor unit is comprised of two motors mounted together and using a range of gains in the current controller, a series of step responses was generated for different values of motor resistance

and inductance. Inputs and outputs were recorded on an oscilloscope.

These results were compared with the model test results and parameter adjustments made until the magnitude of the current step and the dynamics approximately matched the test results. It was found that some adjustments were required to the controller model, including the introduction of a filter to the input signal. The impact of this filter was only visible because of the low inductance of the motor and high bandwidth of the loop. Since the effect on the overall system dynamics is small, these results will not be presented.

ROLLER-SCREW EFFICIENCY

The roller-screw efficiency was investigated by driving one motor in current control mode against the other in position control mode. A force sensor was mounted between the two roller-screws. By comparing the torques and forces in this system with each other, it is possible to measure the roller-screw efficiency. This was found to be of the order of 65%.

During subsequent tests where the frequency response of the motor driving the wedge was investigated, it was found that impact of this parameter could be seen at higher frequencies, because of the losses implied in driving the output mass.

DRIVE TRAIN STIFFNESSES

The drive train stiffness tests consisted of two stages. Firstly the motors were driven against each other using a current demand, with a force sensor mounted between them. This provided both a direct reading of the total stiffness of this portion of the drive in tension and compression and a calibration of the force due to the motor current. Calibration was necessary because once the brake heart is installed, it is not possible to measure the actuation force directly.

The second stage of the testing was to assemble the brake heart and to drive the motors against each other in both tension and compression. Allowing for the stiffness of the force sensor, the value in compression should be essentially the same as previously. In tension, the load path flows through the wedge, including its actuation bearing surfaces, and so the total stiffness is noticeably lower.

Assuming symmetry, this test allowed the values of stiffnesses K_S and K_W (Figure 3) to be set. It also provides a measure of the total free-play in the brake heart.

COMPARISON WITH TEST RESULTS

Because of the potential instability within the system, it was important to take an incremental approach towards validating the model. Consequently, various controllers were tested using hardware ranging from a single motor

with a dummy shaft to the complete prototype. The results were assessed to ensure that they were close enough to those expected before proceeding to the next stage, in order to minimise the risk. A selection of intermediate results is presented here, followed by some comparisons with actual braking time responses. It should be emphasised that the initial results were of most interest for validating the model used for control design. The final validated model has a wider range of uses: e.g. it can be used to perform 'virtual testing' of the system in parallel with the physical tests.

One aspect which is not discussed here in detail, but which is equally important, is the cross-validation of the various models. As an example, it is possible to use a separate linear model for control design, but this should produce the same frequency response as a non-linear model with the friction etc. set to zero. This acts as a check both that the underlying models are both the same, and that the non-linear frequency response analysis is functioning correctly.

MOTOR & ROLLERSCREW ALONE

For initial investigations, a single motor with a solid dummy shaft was used. The next stage was to set up a single motor driving a roller-screw, which is more representative of the complete system.

A variety of cases were tested, but the majority of the work focussed on the frequency responses of a number of motor position controllers. The frequency response was chosen because it is of most relevance to the control law design. Bode plots for two different position controllers are shown in Figures 5 and 6. Figure 5 shows a lower bandwidth controller, where the impact of the current limit is minimal for the amplitudes investigated. Both these results were obtained from driving a preloaded roller-screw, so the effects of friction on the response are clearly seen, particularly at low frequency.

In the second case, the bandwidth achieved by the motor is dependent on the current limit for all the amplitudes. The roll-off in the gain and the 'kink' in the phase plots are clearly visible.

Both these results indicate a good match between theory and practice within the frequency range of interest for the brake system.

POSITION CONTROL OF WEDGE

The main objective of these tests were to validate as far as possible the model being used for control law design. Since the gear ratio between the motor rotation and the linear motion of the output mass is very large, there is very little difference between this arrangement and the previous one. The results are therefore very similar.

FORCE FIGHT TESTS

Because two motors are effectively mounted on the same shaft, small differences in their parameter values can lead to a force fight between them. At the moment, there is no provision in the prototype for measuring the roller-screw forces directly, so it was important to ensure that large margins were available. To ensure that no damage could be done to the mechanical components, several force fight tests were conducted, where the motors were run from a position controller, with a force sensor mounted between the roller-screws. Both frequency and step response data were obtained. This was used for fine-tuning the motor models. This data was then transferred to the model of the complete brake and used as a basis for assessing the loads.

MOMENT CONTROL OF BRAKE

When the brake is under moment control, there are two main considerations in the validation process: the controller stability and the brake performance. Initially, the former is of greatest interest, since any instability which arises could damage the hardware and require an expensive re-work. The dynamics which the brake can achieve are also a result of the controller design. For demonstration of the potential of the design, however, it is also important to demonstrate that the power consumption is the same on the model and the test rig. This then permits the model to be used as an experimental tool in parallel with the hardware.

A few different responses will be shown to illustrate the validity of the existing model. Two input amplitudes will be shown, to give an idea of the effect of non-linearities. For smaller amplitudes, friction is more important, while for larger ones rate and torque limits within the system will dominate.

In all figures, the solid blue lines are measurements, while the dashed red lines are the simulation results. The moment demand has simply been directly injected into the simulation. For practical reasons, the input power is measured at the input to the motor drives. Unfortunately, the signal is heavily filtered by the components and it was not possible to obtain a direct comparison with the model. The results are nevertheless included to substantiate the theoretical claims for the brake. As long as the motor currents and speeds are well matched, then the total input power must also be sufficiently accurate.

Figure 7 shows a 200 Nm step input. After a short time the demand is pulsed to reduce it to 80% of this value, to give an idea of the capability of the brake to perform something similar to an ABS cycle. The motor is accelerated to high speed to bring the brake pad rapidly into contact with the disc. This is the cause of the initial peak in the power curve. The moment is then built up in a controlled manner and held at the desired value. The small oscillations occur once per revolution as the result of significant run-out on the brake disc. It can be seen that once the brake pads are in contact with the disc, the

power required is very small. The steady power drain on the motor drive itself is clearly visible on the plot.

In Figure 8, the same step and reduction to 160 Nm is followed by a slow ramp up to the original value. Again, the desired response is well followed, and model and test results are well matched.

Finally, an input pulse of amplitude 950 Nm is tested (Figure 9). In this case, the motor spends a long time on the software rate limit. This has initially been set to a conservative level while the model is validated, since higher speeds increase the potential for force fight between the two motors. Since the drive train is relatively stiff, small position errors between the two motors can lead to large forces. Although the power response shows neither the initial peak due to motor acceleration nor the very low levels during the actual braking, it can be seen that this braking is achieved with around 60 W input power, validating that the low theoretical power consumption can be achieved in practice. For a longer braking, the input power would in fact reduce with time to the steady state value. The difference between test and simulation at the end of the results is due to a small difference in time between when the model and the rig switch into the controller's 'gap crossing' mode.

From these few cases, it can be seen that the match between the model and the hardware is good. This provides a solid basis for the further development work.

PROGRAMME STATUS

The construction and testing of a second prototype represents a major step forward in the development of the technology. Most importantly, this prototype is designed to operate in the unstable region, to gain the greatest advantage from the wedge principle.

The initial results, some of which have been presented here, are important in that they prove that theoretical benefits of the design are realisable in practice. In particular, it has been shown that the actuator power requirements are low and the dynamics are good.

There is still much to be done, both in terms of exercising the new prototype and of further development. Topics for investigation with the existing prototype include extended testing at extreme values of coefficients of friction and examining the wear on all components.

In the short to medium term, a further prototype is planned which will incorporate the lessons from this one, together with introducing an adjustment mechanism. With more data, both from model and test, it will be possible to re-optimize the drive train, considering both motor sizing and the optimum reduction ratio. Other studies are looking at alternative mechanical arrangements aimed at reducing costs. Failure modes and effects analysis and other safety studies will be addressed on an application by application basis.

CONCLUSION

This paper describes the mathematical model of the brake and its validation against the prototype hardware. It can be seen that the quality of the model is relatively good, both in terms of the stability of the controller and the actuator power requirements.

This demonstrates the validity of the model for analysis of the existing prototype, for 'virtual tests' which can be run in parallel to the physical ones, and for design studies for the next generation of systems.

ACKNOWLEDGMENTS

The authors would like to thank the DLR Institute for Robotics and Mechatronics under Prof. G. Hirzinger for the loan of hardware & software to support this work.

REFERENCES

1. Hartmann, Schautt, Pascucci & Gombert. "eBrake[®] – the mechatronic wedge brake". SAE Paper 2002-01-2582.
2. "DLR RoboDrive. Servomotor for Robotic Applications optimized in Weight and Efficiency". German Aerospace Center DLR, Institute of Robotics and Mechatronics Oberpfaffenhofen, D-82234 Weßling.
3. eStop GmbH. "Electromechanical Brake with Zero Backlash Actuation". Patent WO 02/095257.
4. "Rollengewindegetriebe und Lagerkomponenten, Baueinheiten" INA Sach-Nr. 002-046-431/RGT.

CONTACT

Richard Roberts
eStop GmbH
An der Hartmühle 10
D-82229 Seefeld
Germany
Tel: +49 (0)8152 99 36 12
Fax: +49 (0)8152 99 36 11
e-mail: richard.roberts@estop.de

DEFINITIONS, ACRONYMS, ABBREVIATIONS

C^*	Characteristic brake factor
DLR	Deutsches Zentrum für Luft- und Raumfahrt e.V.
F_A	Axial force on wedge due to abutment
F_{AXIAL}	Axial force on roller-screw bearing
F_B	Force on wedge due to braking
F_{FRICT}	Axial friction force
F_{INT}	Axial force across wedge interface
F_M	Motor axial force
F_N	Normal force across calliper
F_{SCREW}	Roller-screw axial force
F_W	Total axial force on wedge

G_S	Stribeck friction factor
G_V	Factor on viscous bearing friction
i_M	Motor current
J_M	Motor inertia
K_{CAL}	Calliper stiffness
K_S	Roller-screw axial stiffness
k_S	exponent factor for Stribeck friction
K_T	Motor torque constant
K_W	Wedge axial stiffness
k_V	exponent factor for viscous bearing friction
L	Roller-screw lead
L_M	Inductance
M_B	Braking moment
M_W	Mass of wedge
PWM	Pulse Width Modulation
r_B	Effective radius of brake pad
R_M	Resistance
T_{COG}	Motor cogging torque
T_{DAMP}	Motor damping torque
T_{DRIVE}	Driving torque in roller-screw
T_{FRICT}	Friction torque on motor shaft
T_{LOSS}	Torque loss in roller-screw
T_M	Motor electromagnetic torque

T_{SCREW}	Roller-screw torque
V_{IN}	Motor input voltage
x_1	Motor 1 equivalent axial position
x_2	Motor 2 equivalent axial position
x_W	Wedge axial position
α	Wedge angle
η	Roller-screw efficiency
μ_B	Brake pad to disc coefficient of friction
μ_{INT}	Coefficient of friction of wedge interface
μ_R	Coefficient of friction of rollers
ν	Grease viscosity
ω_M	Motor speed
ω_S	Stribeck velocity

APPENDIX

eStop® und eBrake® are registered Trademarks of eStop® GmbH

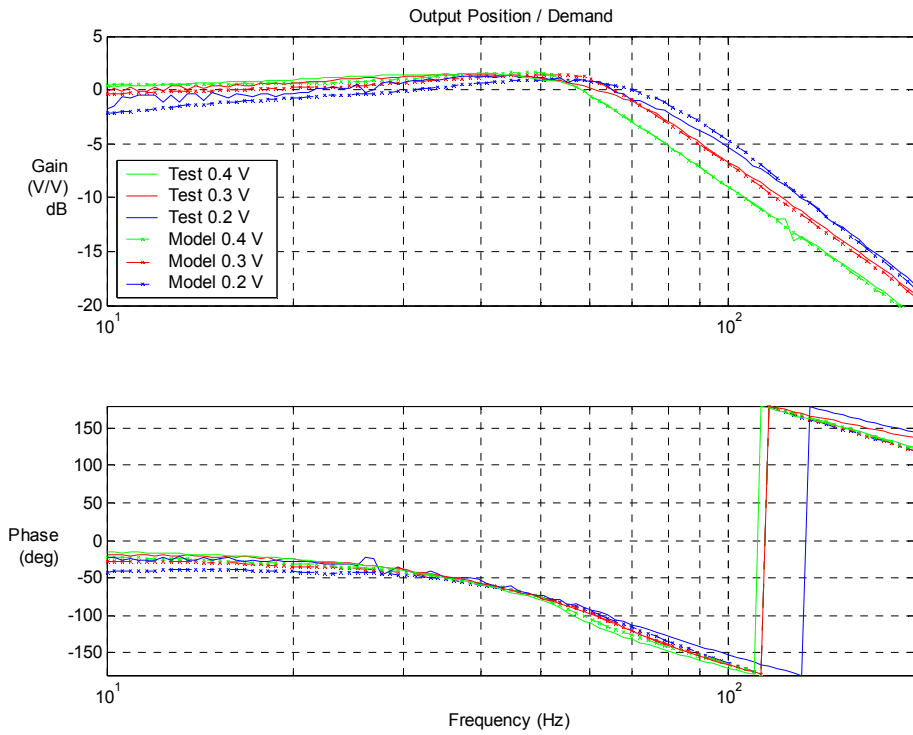


Figure 5: Position Frequency Response, Low Bandwidth Controller

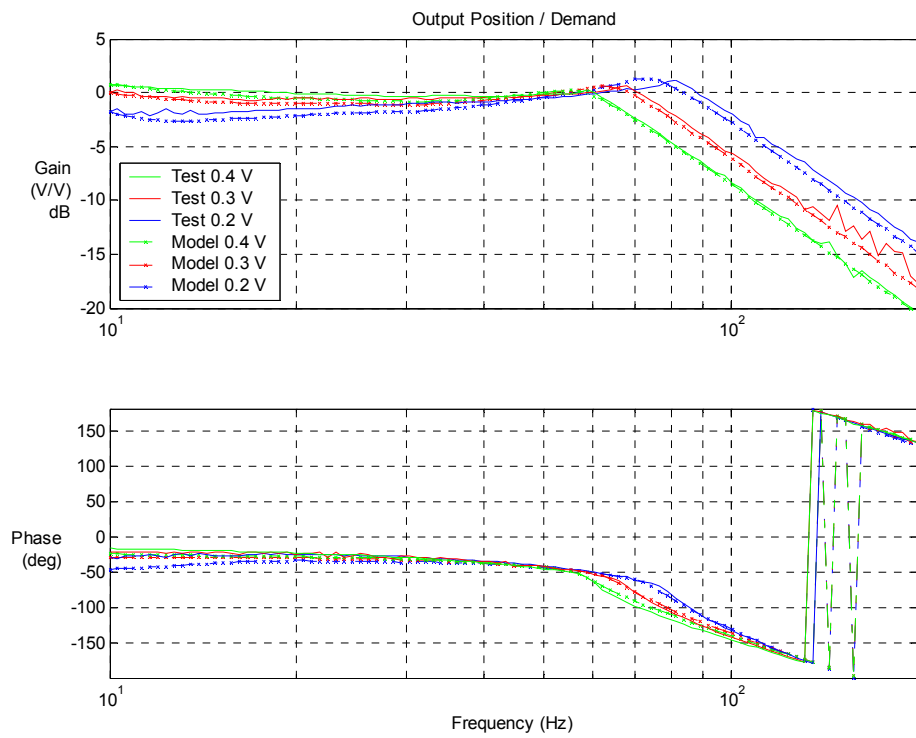


Figure 6: Position Frequency Response, High Bandwidth Controller

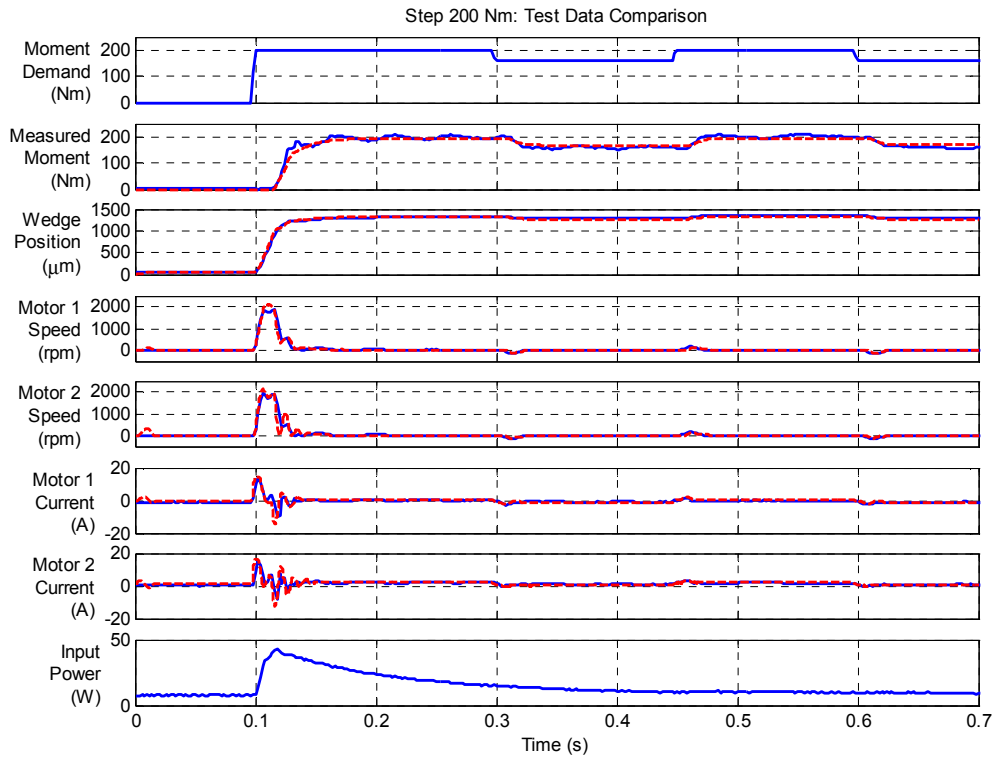


Figure 7: 200 Nm Step in Moment, with Pulses.

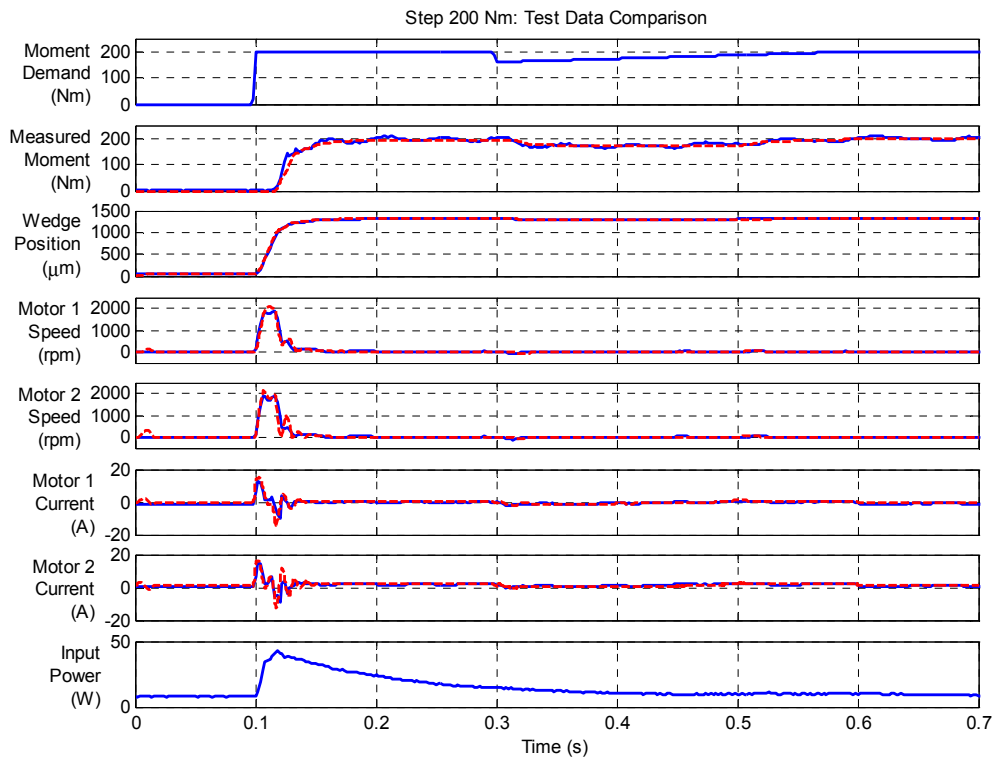


Figure 8: 200 Nm Step in Moment, with Ramp.

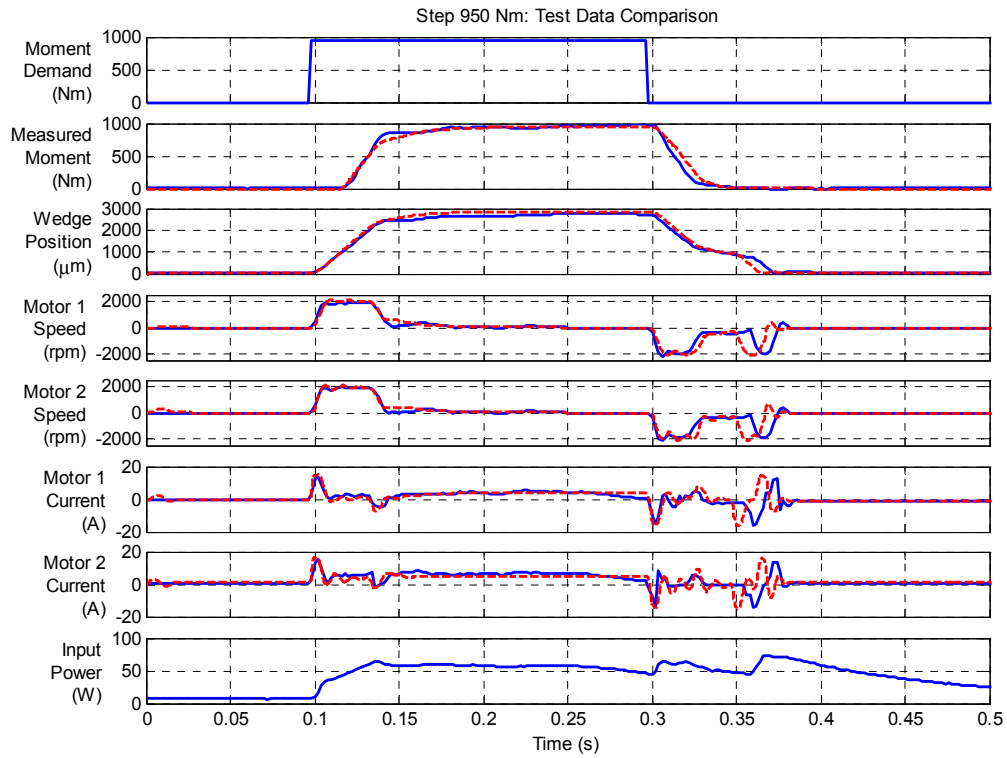


Figure 9: 950 Nm Step Pulse in Moment Demand